ELSEVIER

Journal of Biomechanics 39 (2006) 1686–1701

JOURNAL OF BIOMECHANICS

www.elsevier.com/locate/jbiomech
www.JBiomech.com

A three-dimensional finite element analysis of the combined behavior of ligaments and menisci in the healthy human knee joint

E. Peña*, B. Calvo, M.A. Martínez, M. Doblaré

Group of Structural Mechanics and Material Modelling, Aragon Institute of Engineering Research (I3A), University of Zaragoza, María de Luna, 3, E-50018 Zaragoza, Spain

Accepted 28 April 2005

Abstract

We present here a three-dimensional FE model of the healthy human knee that included the main structures of the joint: bones, all the relevant ligaments and patellar tendon, menisci and articular cartilages. Bones were considered to be rigid, articular cartilage and menisci linearly elastic, isotropic and homogeneous and ligaments hyperelastic and transversely isotropic. Initial strains on the ligaments and patellar tendon were also considered. This model was validated using experimental and numerical results obtained by other authors. Our main goal was to analyze the combined role of menisci and ligaments in load transmission and stability of the human knee.

The results obtained reproduce the complex, nonuniform stress and strain fields that occur in the biological soft tissues involved and the kinematics of the human knee joint under a physiological external load.

Keywords: Finite element method; Biological tissues; Transversely isotropic hyperelastic behavior; Human ligaments; Menisci; Articular cartilages; Human knee joint

1. Introduction

The human knee joint compliance and stability required for optimal daily functions are provided by various articulations and several components like menisci, cartilage, ligaments and muscle forces that allow complex mechanical responses to different types of physiological loads. In particular, and due to the relative incongruence of the articular surfaces, ligaments play a key role in providing passive stability to the joint throughout its whole range of motion. Each ligament provides stability and restrains knee motion in more than one degree of freedom, while the overall joint stability depends on the contributions of the individual ligaments and their interactions. The fully understanding of the role of each individual ligament in motion restraining is essential for the development of an adequate diagnostic and assessment on surgical procedures (Blankevoort and Huiskes, 1991).

Another important multifunctional component of the knee is the meniscus. Menisci are a complex biomechanical system in themselves, with a fundamental role in load transmission, shock absorption, proprioception, improvement of stability and lubrication (Vedi et al., 1999). Load distribution over an incongruent joint surface is effectively redistributed by the menisci by maintaining maximal congruency (Walker and Erkman, 1975). Functionality of the menisci and their role in load transmission have been discussed by Fairbank (1948) and many others (Walker and Erkman, 1975; Fithian et al., 1990; Macnicol and Thomas, 2000).

A proper understanding of knee joint biomechanics is therefore essential to improve the prevention and treatment of its disorders and injuries. Despite the

*Corresponding author. Tel.: +34 976761912; fax: +34 976762578.
E-mail addresses: fany@unizar.es (E. Peña), mdoblare@unizar.es (M. Doblaré).

0021-9290/$ - see front matter © 2005 Elsevier Ltd. All rights reserved.
doi:10.1016/j.jbiomech.2005.04.030

many investigations developed, the exact mechanical behavior of the knee joint and the causes of many of its injures are not completely known yet. This is partially due to inherent limitations of experimental studies such as their high cost, difficulties associated with the obtention of accurate measures of strain and stress and specially the difficult, and sometimes impossible reproduction of certain natural, pathological or degenerative situations. Finite element (FE) models have proved to be able to provide deep insights into the mechanical properties of biological tissues and performance of living organs reducing both cost and time. An appropriately developed finite element model is a powerful tool to predict the effects of the different parameters involved, and to provide information otherwise difficult to obtain from experiments.

It is important to note that the reliability of these models strongly depends on an appropriate geometrical reconstruction and on accurate mathematical descriptions of the behavior of the biological tissues involved and their interactions with the surrounding environment. In this sense, we still need to improve our information about the constitutive behavior of some of the most common biological tissues, such as ligaments, tendons and menisci.

The knee is probably the most studied of all the human joints. However, to our knowledge, there is no published computational analysis that includes menisci, articular cartilages and all the main ligaments (patellar tendon (PT), anterior cruciate (ACL), posterior cruciate (PCL), medial collateral (MCL) and lateral collateral (LCL)) incorporating initial stresses in all of them. The vast majority of previous studies used one-dimensional (1D) representations of the knee ligaments (Bendjaballah et al., 1998; Blankevoort and Huiskes, 1991; Beynnon et al., 1996; Li et al., 1999; Donahue et al., 2002). This approach was proved to be useful for predicting joint kinematics but nonuniform three-dimensional (3D) stresses and strains could not be predicted. Other researchers developed 3D finite element models of individual human ligaments such as the ACL (Hirokawa and Tsuruno, 2000; Pioletti et al., 1998; Song et al., 2004; Limbert et al., 2004) or the MCL (Gardiner et al., 2001). Finally, other papers presented specific computational models of parts of the human knee to discuss different aspects of its biomechanical behavior (Eijden et al., 1986; Abdel-Rahman and Hefzy, 1993). Heegard et al. (1995) developed a 3D model to analyze the human patella biomechanics during passive knee flexion. Beynnon et al. (1996) presented an analytical sagittal plane model of the knee to study how cruciate ligament bundles control joint kinematics. Bendjaballah et al. (1995, 1998) and Jalani et al. (1997) constructed respective nonlinear finite element models of the entire human joint to investigate the biomechanics of the passive tibiofemoral joint in full extension under anterior–posterior drawer forces and internal–external torques. Périé and Hobatho (1998), Li et al. (1999) and Li et al. (2001) considered joint contact stresses and contact areas on the human knee menisci. In all these latter models, ligaments were modelled as nonlinear springs.

We present here a complete 3D model of the healthy human knee joint. This included all the relevant ligaments, menisci and articular cartilages. Different experimental and numerical results were used to validate it initially (Fox et al., 1998; Ahmed and McLean, 2002; Fukubayashi and Kurosawa, 1980; Bendjaballah et al., 1995; Donahue et al., 2002). Once sufficiently validated, our main goal was to analyze the combined role of menisci and ligaments in load transmission and stability. In order to compare with experimental results presented by other authors (Suggs et al., 2003; Lewis et al., 1989; Fu et al., 1999; Yagi et al., 2002; Fox et al., 1998; Ahmed and McLean, 2002), three different load cases were considered. The configuration at full extension served as reference position. A compression load of 1150 N was applied for the three cases that corresponds to the maximal force in the gait cycle obtained by Sathasivam and Walker (1997) at full extension. A load of 134 N was applied in the anterior–posterior direction for the first case. The two other cases corresponded to rotatory examples, with a valgus torque of 10 Nm in the second load case, adding the anterior load of 134 N in the last one.

2. Material and methods

2.1. Knee joint geometry

The geometrical data of the model developed herein were obtained by nuclear magnetic resonance (MRI) for soft tissues and computerized tomography (CT) for bones, with images taken from a normal adult volunteer. The CT and MRI blocks consisted of parallel digital images separated at intervals of 1.5 mm in the sagittal, coronal and axial planes with the knee at 0° flexion.

The contours of the femur, tibia, articular cartilage, menisci and ligaments (patellar tendon, anterior cruciate, posterior cruciate, medial collateral and lateral collateral) were manually identified in each image with the help of M.D.s from the Traumatology Department of the University of Zaragoza. The manual segmentation had an accuracy of 0.3 mm. The locations of the insertion sites were detected and carefully defined by M.D.s from the Traumatology Department (Fig. 1). These lines were transferred into the commercial code I-DEAS v.9 where the main surfaces and solid version of the model were reconstructed with an accuracy of 0.5 mm (Fig. 1c).

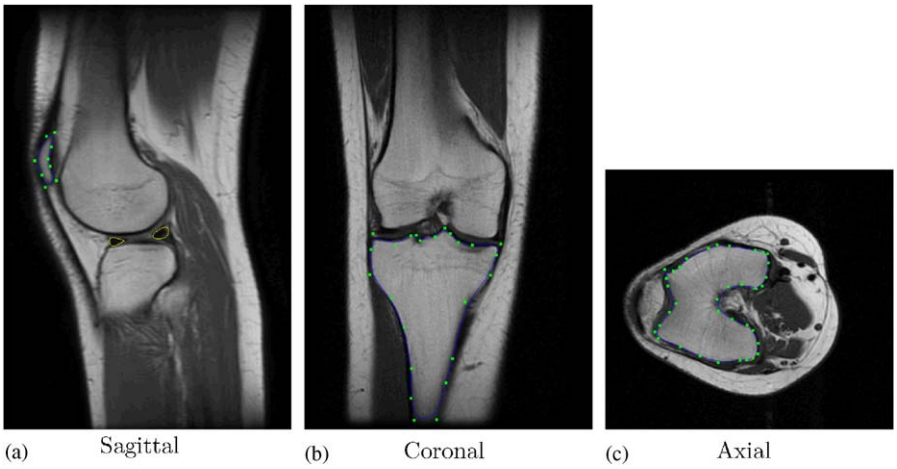

Fig. 1. MR images. (a) Sagittal, (b) Coronal and (c) Axial.

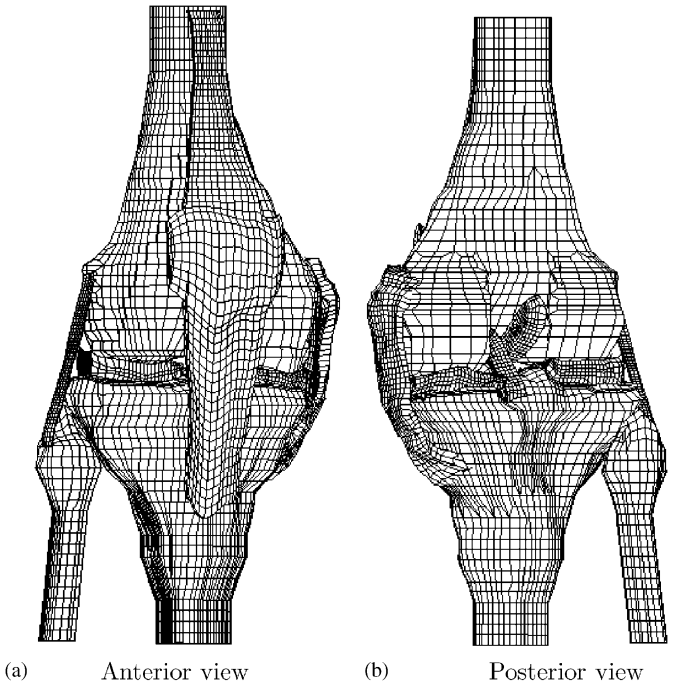

Fig. 2. Finite element model of the knee joint. (a) Anterior view and (b) Posterior view.

Bones were assumed to be rigid in this model (see next section), so only their surface representation was needed. Hexahedral block-structured meshes of the ligaments, menisci and articular cartilages were constructed. A total of 4783 four-node surface elements were used to mesh the bony surfaces and 5195 eight-node brick elements for the meshes of cartilages, menisci and ligaments (Fig. 2). In all the cases, we used trilinear hexahedral elements with a full geometrically nonlinear formulation.

To test the convergence of this mesh, an idealized model was meshed with a doubled mesh density. The differences in peak stresses between the double-densed mesh and the one used in this paper were found to be less than 4%.

2.2. Behavior of hard biological tissues

Since bone stiffness is much higher than that of the relevant soft tissues and its influence in this study was minimal, bones were assumed to be rigid. Each bony structure (femur, tibia, fibula and patella) was therefore represented by a primary node located at its center of rotation at full extension. In the case of the femur this point was located at the midpoint of the transepicondylar line (Daniels, 1990). These nodes, with six degrees of

freedom, controlled the whole kinematics of each bone as rigid body.

2.3. Behavior of soft biological tissues

Menisci and cartilage are hydrated tissues. However, in our case, and considering that the loading time of interest corresponded to that of a single leg stance, and the viscoelastic time constant of cartilage approaches 1500 s (Armstrong et al., 1984), articular cartilage was considered to behave as a single-phase linear elastic and isotropic material with an elastic modulus of $E = 5$ MPa and a Poisson ratio of $v = 0.46$ (Li et al., 2001). This is accurate enough to predict short-term cartilage response as demonstrated by Donzelli et al. (1999), who proved that there are no significant changes in the cartilage contact response shortly after loading. For the same reason, menisci were also assumed to be a single-phase linear elastic and isotropic material with the following average properties: elastic modulus of $E = 59$ MPa and Poisson ratio of $v = 0.49$ (LeRoux and Setton, 2002).

On modelling ligaments, two important assumptions were made. First, no difference in the material behavior between the ligament body and its insertion were considered. Second, material characteristics depending on time, such as viscoelasticity, creep and relaxation were neglected (Hirokawa and Tsuruno, 2000) due again to the high ratio between the viscoelastic time constant of the material and the loading time of interest in this study. We used therefore a transversely isotropic hyperelastic model including the effect of one family of fibers, usually applied to ligaments (Weiss and Gardiner, 2001). The initial direction of the fibers at each point was defined by a unit vector field $\mathbf{a}_0(\mathbf{X})$. Fibers move with the material points of the continuum body. The fiber direction at each time is described by the unit vector field $\mathbf{a}(\mathbf{x}, t)$. Its stretch λ, defined as the ratio between the length of the fiber in the deformed and reference configurations, can be expressed as $\lambda^2 = \mathbf{a}_0\mathbf{C}\mathbf{a}_0$ with $\mathbf{C}$ the Cauchy–Green strain measure $\mathbf{C} = \mathbf{F}^{\mathbf{T}}\mathbf{F}$, being $\mathbf{F}$ the deformation gradient $\mathbf{F} = \partial\mathbf{x}/\partial\mathbf{X}$ with $\mathbf{x}$, $\mathbf{X}$ the coordinates of each point in the current and initial configurations respectively (Holzapfel, 2000).

Due to the well-known difficulties that appear in displacement-based finite elements in the analysis of nearly incompressible materials, a multiplicative decomposition of $\mathbf{F}$ into *volume-changing* (*dilational*) and *volume-preserving* (*distortional*) parts (Flory, 1961) was established as $\mathbf{F} = J^{\frac{1}{3}}\overline{\mathbf{F}}$. With the same objective, we postulated the existence of a unique decoupled representation of the strain-energy density function Ψ such as

$$\Psi = \Psi_{\text{vol}}(J) + \Psi_{\text{iso}}(\overline{\mathbf{C}}, \mathbf{a}_0 \otimes \mathbf{a}_0), \tag{1}$$

where $\Psi_{\text{vol}}(J)$ and $\Psi_{\text{iso}}(\overline{\mathbf{C}}, \mathbf{a}_0 \otimes \mathbf{a}_0)$ are given scalar-valued functions of the jacobian $J = det\mathbf{F}$ and the modified Cauchy–Green tensor $\overline{\mathbf{C}} = J^{-\frac{2}{3}}\mathbf{C}$ respectively, that describe the volumetric and the isochoric responses of the material. The isochoric part Ψ_{iso} of the strain-energy function was divided into an isotropic part (F_1) that corresponds to a Neo-Hookean model and other depending on the collagen fibers (F_2). The volumetric part Ψ_{vol} was considered, in a standard manner for quasi-incompressible materials, as a penalty function of the jacobian (Holzapfel, 2000). We had in turn

$$\Psi = \frac{1}{2D}\ln(J)^2 + C_1(\overline{I}_1 - 3) + F_2(\lambda), \tag{2}$$

where C_1 is the Neo-Hookean constant and D the inverse of the bulk modulus $k = 1/D$ which was chosen for all the ligaments as $k/C_1 = 1000$ (Weiss et al., 2002).

Following physical observations in human ligaments, we assumed that collagen fibers do not support compressive loads. Secondly, the stress–strain relation curves for ligaments have two well-defined parts: an initial curve with increasing stiffness (toe region) and a second part with stiffness almost constant (linear region) (Viidik, 1990). We used the free-energy function (3) earlier proposed by Weiss et al. (1996).

$$\begin{aligned}
&\lambda\frac{\partial F_2}{\partial\lambda} = 0, \quad \lambda < 1,\\
&\lambda\frac{\partial F_2}{\partial\lambda} = C_3(e^{C_4(\lambda-1)} - 1), \quad \lambda < \lambda^*,\\
&\lambda\frac{\partial F_2}{\partial\lambda} = C_5\lambda + C_6, \quad \lambda > \lambda^*,
\end{aligned} \tag{3}$$

where $\overline{I}_1 = tr(\overline{\mathbf{C}})$ is the first invariant of $\overline{\mathbf{C}}$, λ^* is the stretch at which collagen fibers start to be straightened, changing Ψ from exponential to linear, C_3 scales the exponential stress, C_4 is related to the rate of collagen uncrimping and C_5 is the elastic modulus of the straightened collagen fibers. We used the average constants obtained by Gardiner and Weiss (2003) for the MCL in their experimental data. The LCL constants were assumed to be identical to those of the MCL. We fitted the uniaxial stress–strain curves obtained by Butler et al. (1990) for ACL, PCL and PT with those obtained by Weiss getting the associated constants that have been included in Table 1.

The local fiber orientation ($\mathbf{a}_0$) was specified according to the local element geometry (Weiss et al., 1996). The true Cauchy stress tensor, $\boldsymbol{\sigma}$, and the elasticity tensor in the spatial description were obtained in a

Table 1
Material parameters for the ligament stress-free state (MPa)

	C_1	C_2	C_3	C_4	C_5	λ^*	D
MCL	1.44	0.0	0.57	48.0	467.1	1.063	0.00126
LCL	1.44	0.0	0.57	48.0	467.1	1.063	0.00126
ACL	1.95	0.0	0.0139	116.22	535.039	1.046	0.00683
PCL	3.25	0.0	0.1196	87.178	431.063	1.035	0.0041
PT	2.75	0.0	0.065	115.89	777.56	1.042	0.00484

standard manner for compressible hyperelastic materials, see i.e. (Weiss et al., 1996) or (Holzapfel, 2000).

To investigate the effect of the variation of some of the model parameters on the predicted contact pressures and maximal compression and shear stresses, several values of E and v both for articular cartilage and menisci and of the constants of the ligaments cited above were checked.

2.4. Enforcement of initial strains

Biological soft tissues are usually exposed to a complex distribution of "in vivo" residual stresses as a consequence of the continuous growth, remodelling, damage and viscoelastic strains that they suffer along their whole life. These stresses can be relieved by selective cutting of the living tissue and removal of its internal constraints. Their most important aim is to homogenize the final stress distribution at different stages of tissue deformation (Fung, 1993).

In order to describe the current deformation state, we followed the methodology initially proposed by Weiss et al. (1995) to enforce initial strains in hyperelastic soft tissues. Three different configurations were defined: (a) the stress-free state (Ω_{fs}), (b) the reference state in which the material is only under the initial strain (Ω_0) and (c) the current deformed state (Ω). It was assumed that the total deformation gradient tensor corresponding to the current state $\mathbf{F}$ admits a multiplicative decomposition $\mathbf{F}=\mathbf{F}_r\mathbf{F}_0$, where $\mathbf{F}_0$ represents the deformation gradient corresponding to the initial strains and a subsequent unloaded equilibrium step, and $\mathbf{F}_r$ is the deformation gradient that results from applying the external loads to this initial configuration Ω_0.

The initial stress in the reference state, $\boldsymbol{\sigma}_0$, is defined for hyperelastic materials in the standard form, by the strain-energy density function $\Psi_{\Omega_{fs}}$ referred to the stress-free state Ω_{fs}. We assumed that this strain-energy function is modified in the reference state due to the nonlinear behavior of the material and the variation in the fiber direction. The new strain-energy function referred to the unloaded configuration is denoted by Ψ_{Ω_0}.

To introduce initial strains it is necessary to specify the initial strains and obtain $\mathbf{F}_0$ pointwise within the finite element mesh. The total stress corresponding to the current state, $\boldsymbol{\sigma}$, is then computed by

$$\boldsymbol{\sigma}=\frac{2}{J}\mathbf{F}_r\left[\frac{\boldsymbol{\sigma}_0}{2}+\frac{\partial\Psi_{\Omega_0}(\mathbf{C})}{\partial\mathbf{C}}\right]\mathbf{F}_r^T \tag{4}$$

and the elasticity tensor derived in the standard form from the new strain-energy function Ψ_{Ω_0}.

In the case of ligaments and tendons, Gardiner et al. (2001) proposed a relatively easy form to measure length variations along the fiber direction at different points. The concomitant contraction in the perpendicular plane was dictated by the usual incompressibility assumption in biological soft tissues. With this information, they were able to calculate $\mathbf{F}_0$. Initial strains in our model were defined from data available in literature (Blankevoort and Huiskes, 1991), (Li et al., 1999) and (Song et al., 2004) and have been included in Table 2 with the following terminology: a: anterior part of ligament; p: posterior part of ligament; m: medial part of ligament.

Table 2
% Ligament initial strains at full extension

*a*AC	*p*AC	*a*PC	*p*PC	*a*LC	*m*LC	*p*LC	*a*MC	*m*MC	*p*MC
0.06	0.1	0.0	0.0	0.0	0.0	0.08	0.04	0.04	0.03

Initial strains should provoke an autoequilibrated state. However, the initially prescribed values were obtained by optimization techniques from experimental data and do not produce this autoequilibrated state. For this reason, it is necessary to enforce an equilibrium step. Fig. 3 shows the strain distribution for the ligaments after equilibrium but before the application of external loads. Obviously, the initial strains obtained after that equilibrium step are not exactly the prescribed ones. The differences found were all of them under 10% except in the PCL where a small initial strain appeared after equilibrium that Blankevoort and Huiskes (1991) did not consider.

This constitutive model was implemented into the commercial FE code ABAQUS v.6.2 (Hibbit, Karlsson and Sorensen, Inc., 2004) through a Fortran user subroutine. The resulting numerical model was validated with analytical solutions for different states of homogeneous deformation (Calvo et al., 2005), founding an excellent agreement.

2.5. Loads and boundary conditions

Boundary conditions were defined as follows. Each of the horns of the menisci and the external periphery of the medial meniscus, which is joined to the medial collateral ligament, were attached to the tibial plateau, simulating the horn-menisci attachment. Ligaments were attached to bone by establishing the final row of elements at their proximal and distal ends to be composed of the same material than the nearby bone (Gardiner and Weiss, 2003).

Frictionless nonlinear contact was assumed for all the articulations (Murakami, 1990) and 15 potential contact zones were identified: two at the medial zone and two at the lateral (femoral cartilage-meniscus and meniscus-tibial cartilage), four between ligaments (MCL, LCL, ACL and PCL) and femur, four between ligaments and tibia and one between cruciate ligaments and between the femoral cartilage and the retropatellar articular

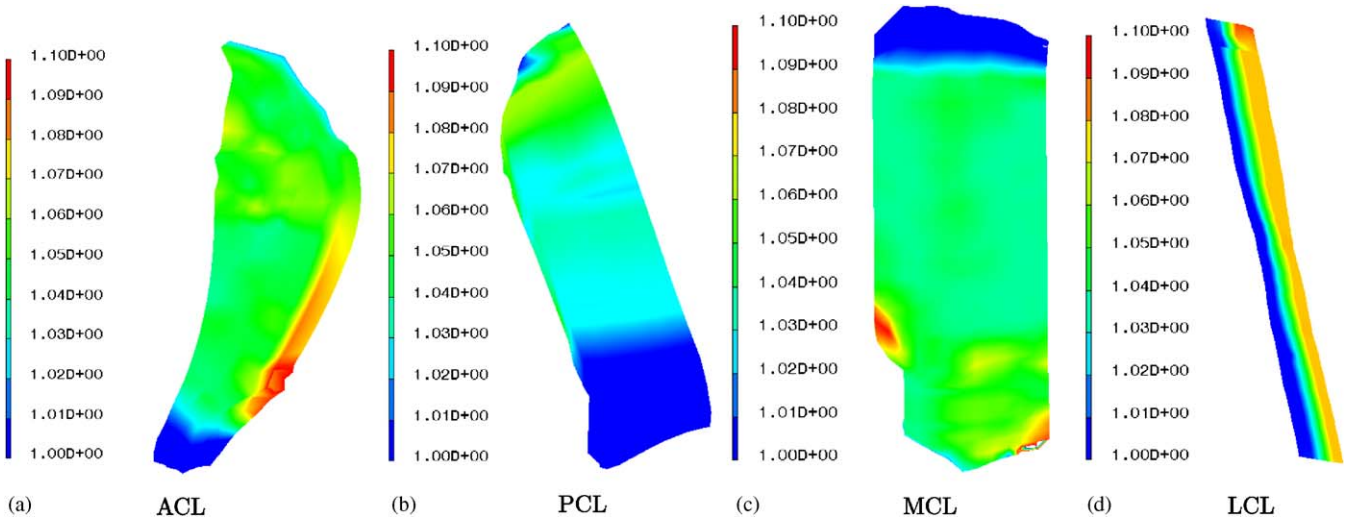

Fig. 3. Initial stretch of the fibers after the equilibrium step and before loading. (a) ACL, (b) PCL, (c) MCL and (d) LCL.

cartilage. Contact conditions in the model were completely general including finite sliding.

The motion of each bone was controlled by the six degrees of freedom of its reference node. In all the analyses, tibia and fibula remained fixed and the flexion–extension was fixed for the femur. The position at full extension served as the reference initial configuration. In order to compare the obtained results with those presented by other authors (Suggs et al., 2003; Lewis et al., 1989; Fu et al., 1999; Yagi et al., 2002; Fox et al., 1998; Ahmed and McLean, 2002), a combined load of 1150 N in compression and 134 N anterior–posterior was applied to the femur in the first example. In the second example, the same compression load of 1150 N was applied together with a valgus torque of 10 Nm, adding the anterior load of 134 N in the third example. Comparing this AP force with the compressive force of 1150 N, this would be equivalent to a friction coefficient of 0.12. This is not however correct since, in general, it is not possible to establish a linear relation between the AP and the compressive force. The load is not only transmitted by the contact surface. On the contrary, the AP force is mainly supported by ligaments and patellar tendon while the compressive force is mainly supported by menisci and articular cartilage.

Table 3
Variation 3of the contact pressure, maximal compression stress and shear stress (MPa) in cartilage with several values of the material parameters of menisci under a compressive load of 1150 N and an anterior tibial load of 134 N

	Young's modulus $E-(\nu=0.46)$			Poisson's ratio $\nu-(E=9$ MPa)		
	5	9	15	0.3	0.4	0.46
Contact pressure	3.45	3.68	4.36	3.33	3.52	3.68
Compression stress	3.61	3.82	4.30	4.20	3.95	3.82
Shear stress	3.06	3.27	3.53	3.99	3.59	3.27

Table 4
Variation of the contact pressure, maximal compression stress and shear stress (MPa) in cartilage with several values of the material parameters of menisci under a compressive load of 1150 N and an anterior tibial load of 134 N

	Young's modulus $E-(\nu=0.49)$			Poisson's ratio $\nu-(E=59$ MPa)		
	20	59	120	0.4	0.45	0.49
Contact pressure	3.20	3.68	5.83	3.33	3.51	3.68
Compression stress	3.78	3.82	4.44	3.57	3.71	3.82
Shear stress	3.41	3.27	3.039	3.23	3.25	3.27

3. Results

3.1. Anterior tibial load

Under the proposed anterior tibial load of 134 N and a compression load of 1150 N, the anterior cruciate ligament supported about 75% of the total anterior load and the medial collateral ligament the rest 25% as secondary stabilizer. The tibial displacements resulted to be 5.2 mm along the anterior direction, 0.56 mm for the medial direction, 0.76° of valgus rotation and 1.6° of internal rotation, Table 5.

Figs. 4a and 5 show the results obtained in different ligaments under this anterior load. A significant tensile stress appeared in the posterior part of the ACL, while a moderate tensile stress was observed in the anterior part.

The highest maximal principal stress took place at the posterior region of the femoral insertion of the ACL, with an average value of 6.5 MPa and a maximum of 15 MPa near the femoral insertion. The obtained results also showed that the PCL was mainly in compression; only the anterior proximal part was tensioned with a value of about 3 MPa. The LCL was also mainly in compression except at the posterior and the femoral and tibial insertions region where the average maximal principal stress was 3.5 MPa. The LCL was tensioned due to the initial strains since during this movement it is mainly relaxed, Table 2. The anterior load produced in the MCL a stress distribution similar to a shear problem, with tension in the anterior–distal and the posterior–proximal parts of the MCL. The maximal principal stress resulted to be 3.5 MPa.

Menisci transferred about 62% of the total axial load (40% the medial meniscus, mainly concentrated

Table 5
Kinematics of the knee in response to a combined compressive load of 1150 N and an anterior–posterior tibial load of 134 N

	Anterior (mm)	Medial (mm)	Distal (mm)	Valgus (°)	Internal (°)
Anterior load	4.75	0.56	−1.10	0.76	1.6
Posterior load	−5.035	−0.02	−0.72	0.48	−0.362

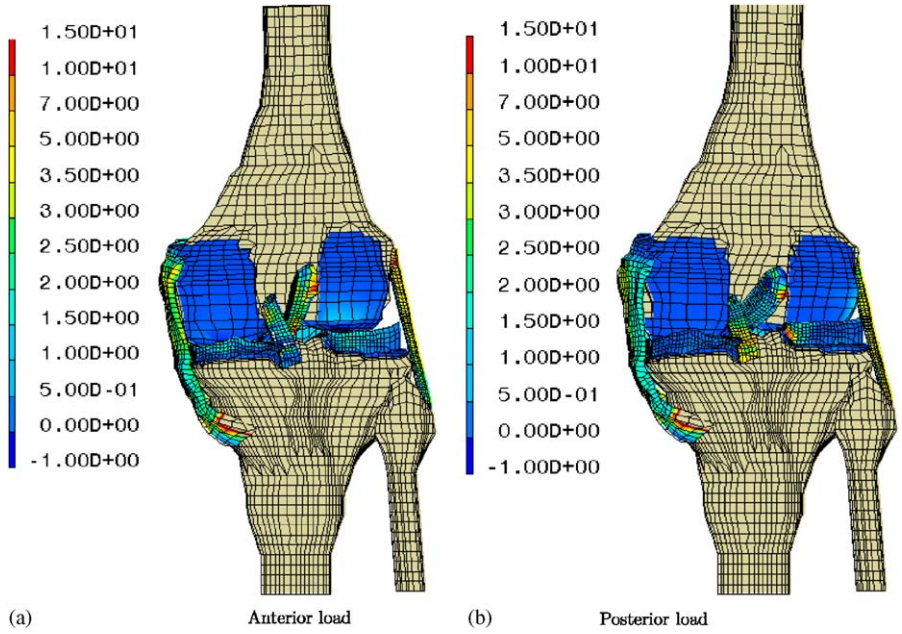

Fig. 4. Maximal principal stresses under anterior and posterior loads (MPa). (a) Anterior load and (b) Posterior load.

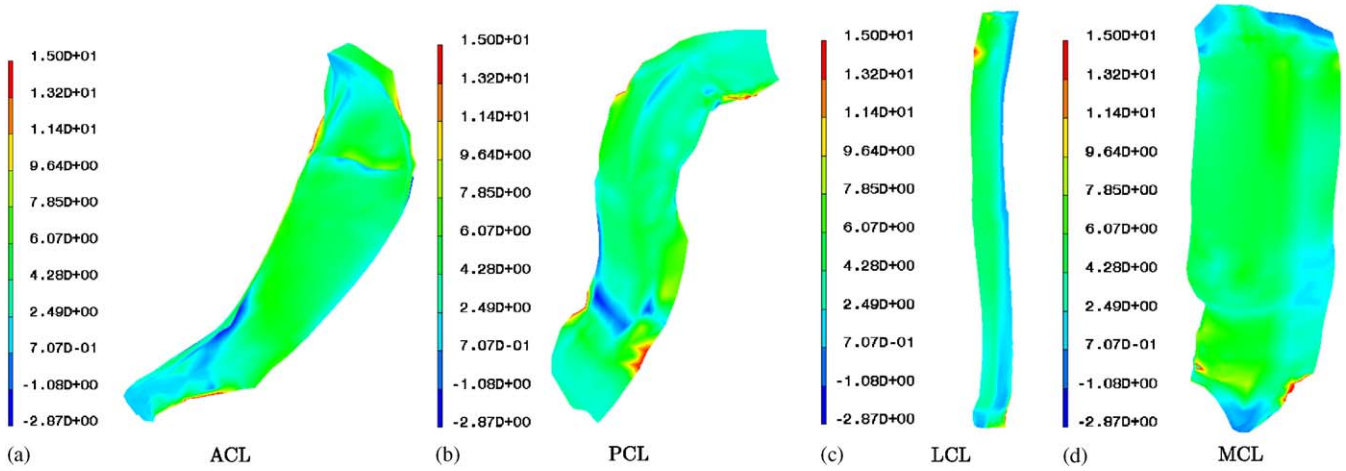

Fig. 5. Maximal principal stresses in the ligaments in response to a compressive load of 1150 N and an anterior tibial load of 134 N (MPa). (a) ACL, (b) PCL (c) LCL and (d) MCL.

on the lateral side (Fig. 6a)). The highest contact pressure took place in the posterior region of the medial meniscus, with a maximum of 3.15 MPa, and in the anterior horn of the lateral meniscus, with 3.68 MPa. Contact stresses were slightly higher in the lateral meniscus as shown in Fig. 6. They basically corresponded to the contact zones between the femoral condyles and the menisci and were very similar to those obtained experimentally by Walker and Erkman (1975).

The femoral cartilage was also in compression with the minimal principal stress (maximal in compression) oriented almost normal to the articular surface, showing higher stresses on the medial condyle with a maximum compressive stress of about −3.11 MPa (Fig. 6d). Similar results were obtained for the tibial cartilage (Fig. 6c). In this case, the compression stress was −2.55 MPa. A summary of these results is presented in Table 6.

Table 6
Summary of the numerical results (MPa) under a compressive load of 1150 N and an anterior tibial load of 134 N with the following terminology: CPMM: contact pressure in medial meniscus, CPLM: contact pressure in lateral meniscus, SMM: compression stress in medial meniscus, SLC: compression stress in lateral meniscus, SMC: compression stress in medial articular condyle cartilage, SLC: compression stress in lateral articular condyle cartilage, SMT: compression stress in medial articular tibial cartilage and SLT: compression stress in lateral articular tibial cartilage

CPLM	CPMM	SLM	SMM	SMC	SLC	SMT	SLT
3.15	3.68	3.82	2.15	2.68	3.11	2.19	1.76

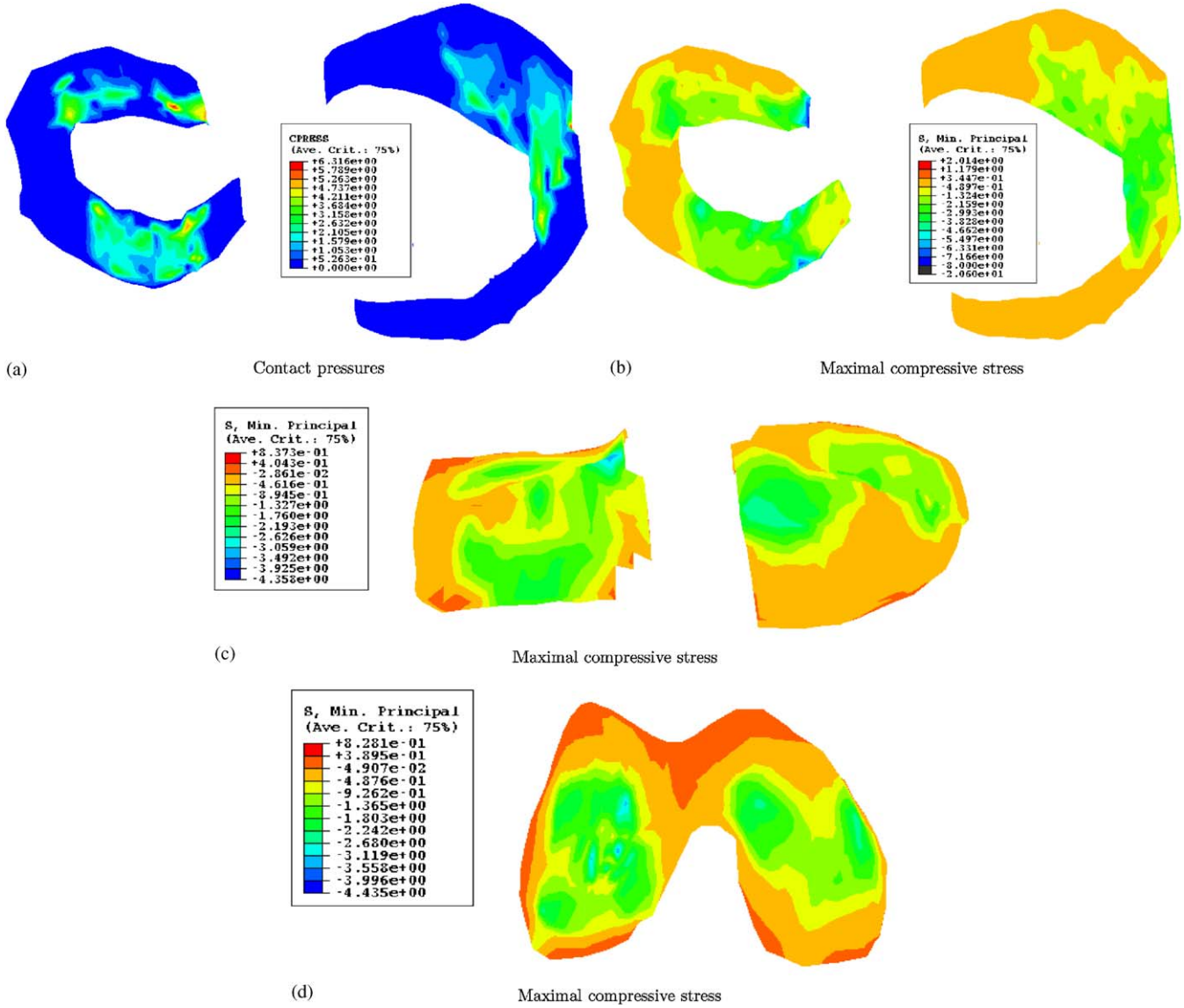

Fig. 6. Stresses in menisci and articular cartilages in response to a compressive load of 1150 N and an anterior tibial load of 134 N (MPa). (a) Contact pressures, (b) Maximal compressive stress, (c) Maximal compressive stress and (d) Maximal compressive stress.

Our calculation detected a contact area of 359 mm^2 at the medial plateau under 1150 N of compressive load. With respect to the contact areas in the femoral cartilages, a summary of the results is presented in Table 7.

Both the Young's modulus and Poisson ratio of articular cartilage were shown to affect the predicted contact pressures, maximal compression and shear stresses in the cartilage (see Table 3). When the Young's modulus decreased from 9 to 5 MPa, the contact pressure also decreased to 3.45 MPa, and when the Young's modulus was increased to 15 MPa, the contact pressure increased up to 4.36 MPa. A similar influence was also detected in both maximal compression and shear stresses. When the Poisson ratio was decreased from 0.46 to 0.4 MPa and 0.3, the contact pressure only decreased to 3.52 and 3.33 MPa, respectively. On the contrary, when the Poisson ratio was decreased, the compression and shear stresses increased.

Variations of the material properties of the menisci produced similar changes in the contact pressure and the maximal compression and shear stresses in the articular cartilage (Table 4). For example, increasing the Young's modulus from 59 to 120 MPa caused a variation of the contact stress from 3.68 to 5.83 MPa, the maximal compression stress changed from −3.82 to −4.44 MPa and the shear stress decreased from 3.27 to 3.039 MPa. Changing the Poisson ratio of the menisci from 0.49 to 0.4 produced relatively low changes in the results. The contact pressure, maximal compression stress and shear stress only decreased 10%, 7% and 0.006%, respectively (Tables 3 and 4).

Table 7
Summary of the obtained contact areas (mm^2) under a compressive load of 1150 N and an anterior tibial load of 134 N with the following terminology: MMCF: contact area between medial meniscus and femoral condyle, MLCF: contact area between lateral meniscus and femoral condyle, CTMCF: contact area between femoral condyle and medial articular cartilage, CTLCF: contact area between femoral condyle and lateral articular cartilage

MMCF	MLCF	CTMCF	CTLCF
210	239.9	149.8	203.2

In this case, the tibial displacement resulted to be 4.75 mm along the anterior direction, 0.56 mm along the medial direction, 0.76° of valgus rotation and 1.6° of internal rotation. An increment of the initial strains of 10% with respect to the actual initial strains gave rise to a decrease of the displacements. The displacement were 4.36 mm along the anterior direction, 0.51 mm along the medial direction, 0.69° of valgus rotation and 1.53° of internal rotation. On the contrary, when the initial strains decreased the same 10%, the changes were more relevant. The tibial displacements resulted to be 6.1 mm along the anterior direction, 0.70 mm along the medial direction, 0.98° of valgus rotation and 1.9° of internal rotation. Fully removing the initial strains provoked an unphysiological movement of the knee under the proposed anterior tibial load of 134 N and compressive load of 1150 N. The tibial displacement resulted to be 7.1 mm along the anterior direction, 0.86 mm along the medial direction, 1.24° of valgus rotation and 7.4° of internal rotation.

3.2. Posterior tibial load

Figs. 4b and 7 show the results obtained in our finite element analysis under the proposed posterior tibial load of 134 N and a compression load of 1150 N. Now,

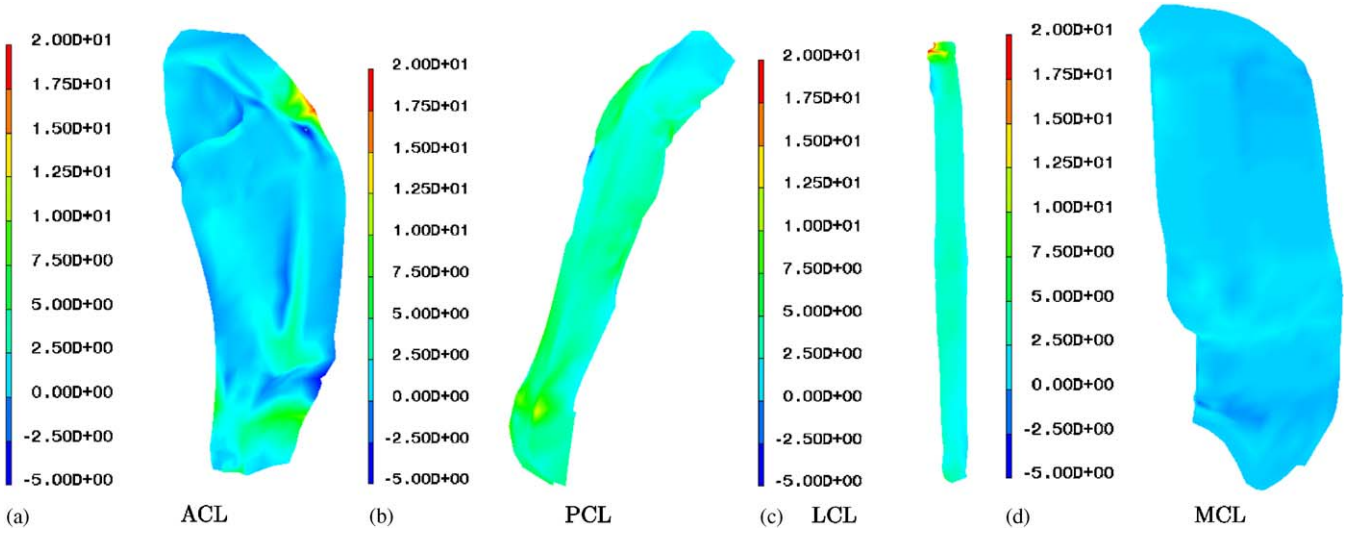

Fig. 7. Maximal principal stresses in the ligaments in response to a compressive load of 1150 N and a posterior tibial load of 134 N (MPa). (a) ACL, (b) PCL, (c) LCL and (d) MCL.

the posterior cruciate ligament supported about 79% of the total anterior load and the lateral collateral ligament the rest 21%. A significant tensile stress appeared in the posterior and medial anterior parts of the PCL. The highest maximal principal stress took place at the posterior region of the tibial insertion of the PCL, with an average value of 7 MPa and a maximum of 15 MPa near the tibial insertion. There is no equivalent result in the literature. The results showed that the ACL was mainly relaxed; only the anterior part of the femoral insertion was tensioned with values over 3.7 MPa. The LCL was also in tension, with a maximum principal stress of 4.5 MPa. The posterior load produced relaxation in MCL except at the insertions. The maximum principal stress in this ligament was 2.57 MPa.

The menisci transferred about 75% of the total axial load (60% the medial meniscus), mainly concentrated on the posterior region. The maximum contact pressure took place in the posterior region of the medial meniscus, with 4.1 MPa, and in the posterior horn of the lateral meniscus with a maximum of 4.81 MPa. The femoral cartilage was also mainly in compression with the minimum principal stress on the medial condyle of about −4.5 MPa.

Table 8
Kinematics of the knee in response to the combination of a compressive load of 1150 N and a valgus torque of 10 Nm and anterior load of 134 N

Anterior (mm)	Medial (mm)	Distal (mm)	Valgus (°)	Internal (°)	
Valgus torque of 10 Nm	2.13	0.717	−1.37	2.62	5.87
Anterior load of 134 N and valgus torque of 10 Nm	4.81	0.25	1.17	1.86	7.2

3.3. Rotatory load

The application of a 10 Nm valgus torque induced a valgus rotation of 2.62°, accompanied by an internal tibial rotation of 5.87°, as observed by other authors (Gardiner et al., 2001), and an anterior translation of 2.13 mm (see Table 8). The MCL provides primary restraint to valgus rotation so, the highest maximal principal stress took place in this ligament. Stress and strain were non-uniformly distributed over the MCL. The highest stress occurred in the posterior proximal region with a value of 5.3 MPa while the lowest appeared in the anterior region. A "buckling" effect (Fig. 8) appeared in the PCL and LCL. On the contrary, the medial part of the ACL was tensioned with a value of 2.65 MPa.

The application of a 10 Nm valgus torque decreased the transferred load by the medial meniscus, that became about 43% of the total axial load (Fig. 9a). The highest contact pressure took place in the lateral meniscus, with a maximum value of 5 MPa and an average of 3.81 MPa. The minimal principal stress (maximal compression) took place in the lateral meniscus with a value of −8.4 MPa (Fig. 9b). The highest minimal principal stress in the femoral cartilage was observed in the lateral condyle with a value of −4.12 MPa, while in the medial condyle this value was of −1.62 MPa (Fig. 9d). Similar results were obtained in the tibial cartilage. The highest minimal principal stress appeared in the lateral tibial plateau with a value of −3.15 MPa, whereas in the medial tibial plateau this minimal principal stress was of −1.79 MPa (Fig. 9c).

The anterior tibial load decreased the valgus rotation to 1.86° and increased the internal tibial rotation to 7.2°. Logically, the anterior tibial displacement grew up to 4.81 mm (Table 8). The highest maximal principal stress in the MCL increased up to 5.6 MPa. Since the ACL is the principal restraining structure for anterior loads, the

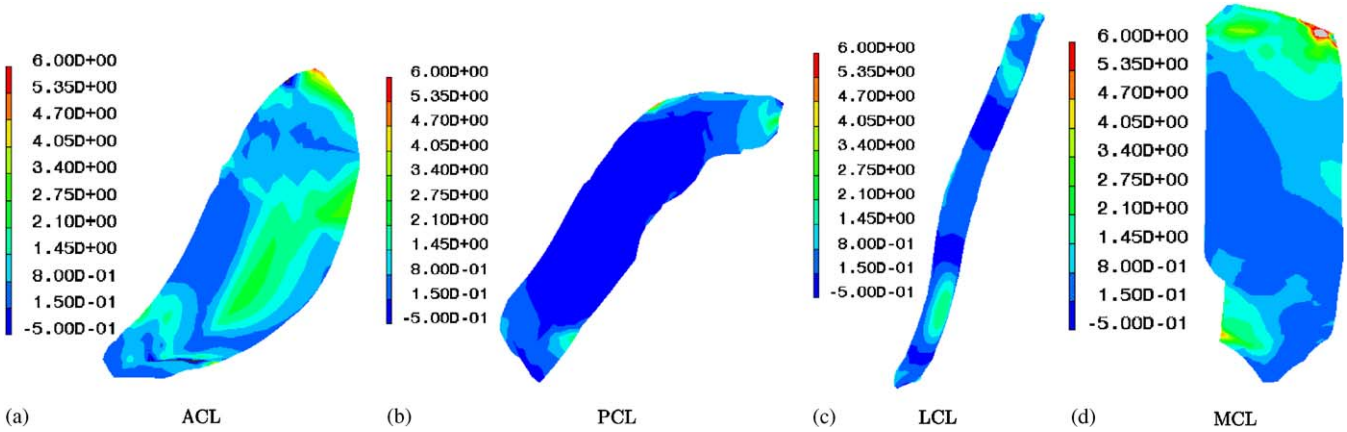

Fig. 8. Maximal principal stresses in the ligaments in response to a compressive load of 1150 N and a valgus torque of 10 Nm (MPa). (a) ACL, (b) PCL, (c) LCL, and (d) MCL.

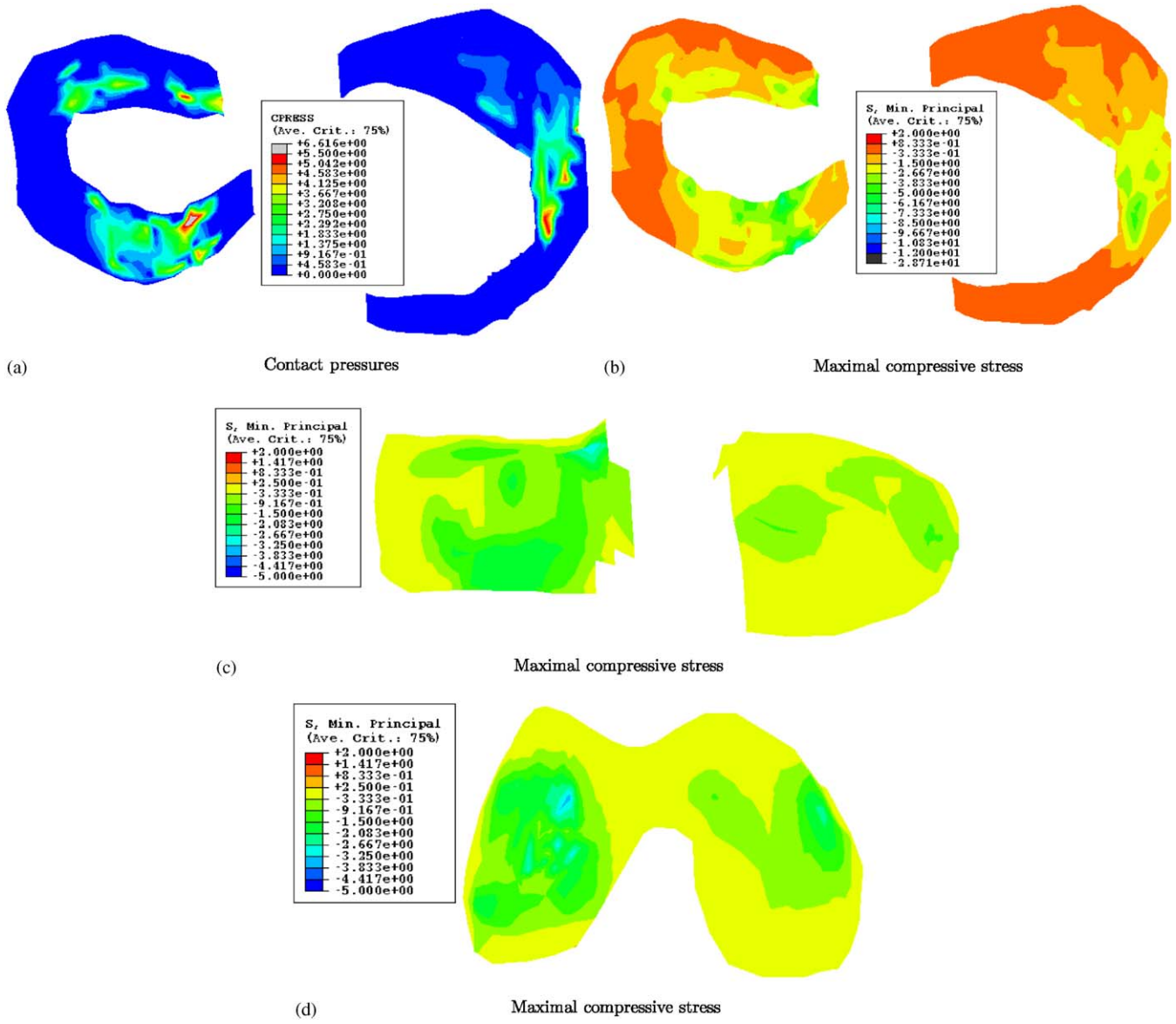

Fig. 9. Stresses in menisci and articular cartilages under valgus rotation (MPa). (a) Contact pressures, (b) Maximal compressive stress, (c) Maximal compressive stress and (d) Maximal compressive stress.

maximum principal stress in this ligament resulted 17 MPa and took place at the posterior region of the femoral insertion. In this case, "buckling" was observed only in the posterior region of the PCL and LCL, resulting in a decrease of the maximum principal stress. In the anterior region, those ligaments were tensioned due to coupling between anterior movement and valgus rotation.

Menisci transferred about 45% of the total axial load (30% the medial meniscus), mainly concentrated on the posterior region. The maximal contact pressure took place in the anterior region of the lateral meniscus, with 6.0 MPa and in the posterior horn of the medial meniscus with 3.81 MPa. The femoral cartilage was also mainly in compression with a maximum compressive stress of about −4.53 MPa in the lateral condyle (Fig. 10).

4. Discussion

In this paper we present a complete 3D model of the healthy human knee joint. This includes all the relevant ligaments, menisci and articular cartilages. Femur and tibia were considered to be rigid, articular cartilage and menisci linearly elastic, isotropic and homogeneous and ligaments were modelled as hyperelastic transversely isotropic. Initial strains in all the ligaments were considered. This model was validated using experimental and numerical results obtained by other authors

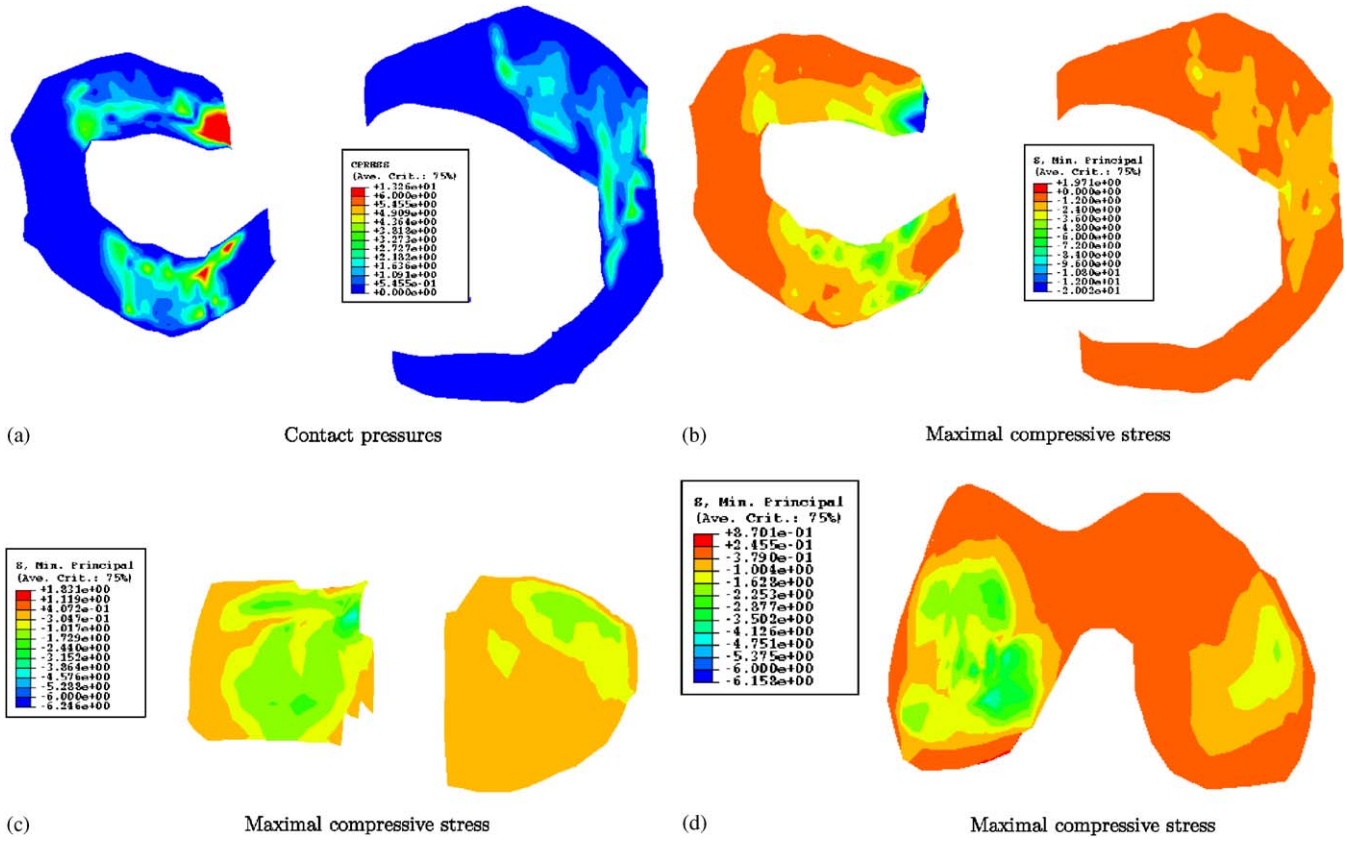

Fig. 10. Stresses in menisci and articular cartilages under valgus rotation and an anterior tibial load (MPa). (a) Contact pressures, (b) Maximal compressive stress, (c) Maximal compressive stress and (d) Maximal compressive stress.

(Fox et al., 1998; Ahmed and McLean, 2002; Fukubayashi and Kurosawa, 1980; Bendjaballah et al., 1995; Donahue et al., 2002). Our main goal was to analyze the combined role of menisci and ligaments in load transmission and stability.

To our knowledge, there is no study in the literature based on a complete knee joint model that includes menisci and articular cartilages and the main ligaments (patellar tendon, anterior cruciate, posterior cruciate, medial collateral and lateral collateral) with pretension in all them. Gardiner and Weiss (2003) developed a finite element model of the MCL to study its 3D stress–strain behavior under valgus loading. The strain distribution in the human MCL under valgus knee loading was measured experimentally and predicted using a subject-specific FE model at three different knee flexion angles. Gabriel et al. (2004) determined "in situ" forces between the two bundles of the ACL with the knee subjected to anterior tibial and rotatory loads. Hirokawa and Tsuruno (2000) developed a 3D model of the ACL that they used to study the strain and stress distributions in the ACL during knee flexion. Limbert et al. (2004) proposed a 3D finite element model of the human ACL. This model was used to simulate clinical procedures such as the Lachman and drawer tests. In all these studies, the finite element model incorporated only one ligament without considering the menisci nor articular cartilages.

Other authors analyzed the distribution of contact pressures and compression stresses in menisci and articular cartilages (Bendjaballah et al., 1995; Périé and Hobatho, 1998; Li et al., 1999). Bendjaballah et al. (1995) only considered a compressive load and modelled the ligaments as nonlinear springs. Peña et al. (2005) presented a 3D model of the knee considering the ligaments as isotropic.

In order to compare our results with those presented by other authors (Suggs et al., 2003; Lewis et al., 1989; Fu et al., 1999; Yagi et al., 2002; Fox et al., 1998; Ahmed and McLean, 2002), a combined compression load of 1150 and 134 N anterior–posterior loads were applied to the tibia in the validation examples. Comparisons between published data and the here predicted kinematics under similar conditions demonstrated its good performance and accuracy. For example, under a posterior tibial load of 134 N and at full extension, Fox et al. (1998) obtained 5.38 mm of posterior displacement and 0.52° of internal rotation in their model with only the ACL. Similar results were obtained in our model: 5.35 mm of posterior

displacement and 0.36°. These results were lower probably due to the inclusion of all ligaments and menisci.

Under an anterior tibial load of 134 N and, at full extension, our model predicted an anterior tibial translation of 4.75 mm. Gabriel et al. (2004) obtained a tibial displacement of 5.0 mm under the same load. Fu et al. (1999) reported an anterior tibial displacement of 5.2 mm. These higher values are probably due to the non-inclusion of the compressive load. Song et al. (2004) obtained 4.6 mm for the anterior displacement, 0.45 mm for the medial, 0.4° for the valgus rotation and 1° for the internal rotation. Our model predicted similar displacements: 4.75 mm of tibial displacement, 0.48° of valgus rotational and 1.6° of internal rotation. On the contrary, Yagi et al. (2002) obtained a value of 4.16 mm with only the ACL, but with the inclusion of the posterior capsule that decreases the global displacement.

The results obtained in ligaments showed high stresses at full extension. This is essentially due to the large sagittal plane rotation of the femoral insertion of the ACL. This was also observed experimentally by Yamamoto et al. (1998) that used photoelasticity to track the strains at the surface of the ACL. Our results also showed a significant tensile stress on the posterior part of the ACL and a moderate tensile stress on the anterior part. Song et al. (2004) obtained 6.9 MPa in the posterolateral bundle of the ACL and 24 MPa in its femoral insertion. Similar results were obtained here: the maximum principal stress took place at the posterior region of the femoral insertion of the ACL, with an average value of 6.5 MPa and a maximum of 15 MPa near the femoral insertion. They obtained that the stress in the middle region of the postero-lateral bundle ranged from 6.1 to 6.9, while those near the tibial insertion site ranged from 1.6 to 6.2 MPa. The corresponding stresses for the antero-medial bundle ranged from 4.7 to 6.2 MPa and 2.6 to 5.3 MPa, in the middle region and near the tibial insertion site. We obtained that the stress in the central region of the posterior bundle ranged from 4.8 to 7.5 MPa and in the tibial insertion the maximal principal stress ranged from 0.7 to 4.5 MPa. The maximal principal stress in the central region of the anterior part and the tibial insertion ranged in our results from 4.8 to 6.5 MPa and 6.07 to 7.85 MPa, respectively. The anterior load produced a stress distribution in the MCL similar to a shear problem, with tension in the anterior–distal and posterior–proximal parts. Similar results were obtained by Hull et al. (1995) in their work, were they measured the strain distribution in the MCL to determine the single and combined external loads most likely to cause injury. Due to the location of the tibial insertion of the PCL, during an anterior displacement of the knee, the tibia pushes the PCL and provokes bending. This implies that some regions of the PCL relax (see Fig. 5b). Since the initial strain of the PCL considered by Blankevoort and Huiskes (1991) was null, the above relaxation implies the low compression in the PCL that can be observed in Fig. 5b. This could mean that the initial strain distribution of the PCL obtained by Blankevoort and Huiskes (1991) is not completely correct and a initial tension would have been considered in the model.

Different authors have used numerical techniques to analyze the distribution of contact pressures and compression stress in menisci and articular cartilage in the healthy knee joint (Bendjaballah et al., 1995; Périé and Hobatho, 1998; Li et al., 1999). Bendjaballah et al. (1995) considered a compression load of 1300 N over the femur and found that the compression stress on the meniscus varied from −1 to −4 MPa in the external and internal periphery, respectively, for the healthy joint. Similar results were obtained in this paper, i.e. a compression stress on the meniscus of −3.82 MPa in the lateral menisci. Donahue et al. (2002) obtained similar results with a maximum contact pressure of 3.46 MPa in the medial meniscus for the healthy joint coincident with experimental results. As shown in Table 2, similar results were obtained in this work. We found that the contact pressure on the articular cartilage was about 3.18 MPa. Fukubayashi and Kurosawa (1980) measured the contact area of the knee joint. Under an axial compressive load of 1000 N, the contact area at the medial plateau of the knee was $300 \pm 80\,\mathrm{mm}^2$. Our calculation showed a contact area of $359\,\mathrm{mm}^2$ at the medial plateau under 1150 N.

Finally, our model was used to study the role of the ligaments and menisci in the stability of the human joint under rotatory loads. In the rotatory examples, a combined compression load of 1150 N with a valgus torque of 10 Nm and combined compression load of 1150 N, valgus torque of 10 Nm and a 134 N anterior load were applied.

Different studies have showed that the MCL provides a primary restraint to valgus rotation and a secondary restraint to external rotation and anterior and posterior translations (Woo et al., 1999). This work supports this conclusion. The maximum principal stress took place in this ligament. Under valgus rotation the highest stress in the MCL occurred near the femoral insertion. Clinical observations of injury patterns confirm that this region is the most common location of injuries in the MCL (Kawada et al., 1999). Previous experimental (Gardiner et al., 2001; Arms et al., 1995; Hull et al., 1995) and computational (Gardiner and Weiss, 2003) studies also supported this result. Gardiner and Weiss (2003) obtained a valgus rotation of $3.2 \pm 0.8°$ under a 10 Nm valgus torque in their experimental study. When an anterior tibial load was applied, the maximum principal stress in the MCL increased due to the function of this ligament as a secondary restrainer under anterior displacements. An interesting finding of our study is

that the anterior tibial load decreased the valgus rotation from 2.62° to 1.86° and increased the internal rotation due to coupling between the anterior displacement and internal rotation. We can compare our results under valgus rotation of 10 Nm with the experimental ones obtained by Gardiner et al. (2001). They found that the highest strains appeared in the proximal region of the MCL with values of 0.079% and 0.094% in the central and posterior regions, respectively. The strain was 0.029%, 0.04% and 0.036% in the anterior, central and posterior regions of the distal part. We obtained similar results, the maximum principal strain resulted in the proximal region of the MCL with values of 0.11% and 0.081% in the posterior and central parts, respectively. The strains in the distal part were 0.018%, 0.038% and 0.042% in the anterior, central and posterior regions respectively.

A valgus rotation of 10 Nm leaded to an important increase of the contact pressures in the lateral menisci. This effect is due to the non-symmetrical load distribution. The contact area at the medial plateau of the knee decreased up to 286 mm^2. Similar results were obtained by Bendjaballah et al. (1997). In their work, they obtained that a valgus moment of 10 Nm decreased the load transmission of the medial meniscus until 35%. Our corresponding result was 43%.

Under valgus rotation only, the maximum compression became lower in the lateral meniscus and corresponding femoral condyle with values of 7.45 and 4.53 MPa. On the contrary, when the valgus rotation and anterior load were applied, the maximum compression stresses were 8.4 and 4.12 MPa, respectively.

Increasing the Young's modulus of the articular cartilage leads to a substantial rise in contact pressures, maximal compression and shear stresses inside the cartilage, see Table 3. On the contrary, a reduction of the value of the Poisson ratio of the articular cartilage increases the maximal compression and shear stress, but decreases the contact pressure. Our results demonstrated that the contact stress is more sensitive to the Young's modulus of the menisci than that of articular cartilage while shear stresses are more sensitive to the Young's modulus and Poisson ratio of the articular cartilage, Table 4.

Kinematic results are strongly dependent on the distribution of initial strains. Without initial strains we got an unphysiological movement (especially the anterior displacement and external rotation). The results showed that high initial strains provoke an overconstraint of the kinematics. On the contrary, decreasing the initial strains increases all displacements and rotations. The kinematics is more depend-ent upon the initial strains than upon the constant parameter of the ligaments. An increase or decrease of initial strains of about 10% caused changes in the kinematics as large as 18%.

Several limitations of the here described model have in any case to be considered. First of all, the results were obtained for a static model of the full extension position of the knee joint. It would be important to study how different joint angles modify the contact areas in the menisci and the stresses in ligaments. Second, the menisci were assumed to be composed by a single-phase linear elastic and isotropic material. Several authors have found that the meniscus is much stiffer in circumferential direction, which could have some influence in the results (Proctor et al., 1989; Spilker et al., 1992; Fithian et al., 1990). Third, much of the proposed model is dependent upon data from other papers that do not correspond to a specific subject. For this reason, the results should be considered with caution. In addition, our results depend on the load values used of 1150 N. The 1150 N load corresponds to the maximal force in the gait cycle obtained by Sathasivam and Walker at full extension. Obviously, for a different load, the contact area and pressure and the kinematics of the knee would change. Finally, the viscoelastic properties of ligaments and meniscus were not considered, although this aspect does not seem to be much relevant in this analysis.

In spite these limitations, the obtained results resulted close to experimental ones, demonstrating that subject-specific FE models can predict the complex, nonuniform stress and strain fields that occur in biological soft tissues and the kinematics of the human knee joint. Our model also makes clear the importance of the combined role of menisci and ligaments in the stability of the joint as primary or secondary restrainers.

Acknowledgements

The authors gratefully acknowledge the research support of the Spanish Ministry of Science and Technology through the research project DPI2003-09110-C02-01 and the Spanish Ministry of Health through the National Network IM3 (Molecular and Multimodal Medical Imaging, Associated Partner, 300 + +, 2003–2005).

References

Abdel-Rahman, E., Hefzy, M.S., 1993. A two-dimensional dynamic anatomical model of the human knee joint. ASME Journal of Biomechanical Engineering 115, 357–365.

Ahmed, A., McLean, C., 2002. In vitro measurement of the restraining role of the anterior cruciate ligament during walking and stair ascent. ASME Journal of Biomechanical Engineering 124, 768–779.

Arms, S., Boyle, J., Johnson, R., Pope, M., 1995. Strain in the medial collateral ligament of the human knee: an autopsy study. Journal of Biomechanics 29, 199–206.

Armstrong, C., Lai, W., Mow, V., 1984. An analysis of the unconfined compression of articular cartilage. ASME Journal of Biomechanical Engineering 106, 165–173.

Bendjaballah, M.Z., Shirazi-adl, A., Zukor, D.J., 1995. Biomechanics of the human knee joint in compression: reconstruction, mesh generation and finite element analysis. Knee 2, 69–79.

Bendjaballah, M.Z., Shirazi-adl, A., Zukor, D.J., 1997. Finite element analysis of human knee joint in varus-valgus. Clinical Biomechanics 12, 139–148.

Bendjaballah, M.Z., Shirazi-adl, A., Zukor, D.J., 1998. Biomechanical response of the passive human knee joint under anterior–posterior forces. Clinical Biomechanics 13, 625–633.

Beynnon, B., Yu, J., Huston, D., Fleming, B., Johnson, R., Haugh, L., Pope, M., 1996. A sagittal plane model of the knee and cruciate ligaments with application of a sensitivity analysis. ASME Journal of Biomechanical Engineering 118, 227–239.

Blankevoort, L., Huiskes, R., 1991. Ligament-bone interaction in a three-dimensional model of the knee. ASME Journal of Biomechanical Engineering 113, 263–269.

Butler, D.L., Sheh, M., Stouffer, D., Samaranayake, V., Levy, M., 1990. Surface strain variation in human patellar tendon and knee cruciate ligaments. ASME Journal of Biomechanical Engineering 39, 38–45.

Calvo, B., Martinez, M., Doblaré, M., 2005. On solving hyperelasticity with the natural element method. International Journal of Numerical Method Engineering 62, 159–185.

Daniels, D.M., 1990. Knee Ligaments: Structure, Function, Injury and Repair. Raven Press, New York.

Donahue, T.L.H., Hull, M.L., Rashid, M.M., Jacobs, R.C., 2002. A finite element model of the human knee joint for the study of tibio-femoral contact. ASME Journal of Biomechanical Engineering 124, 273–280.

Donzelli, P., Spilker, R.S., Ateshian, G.A., Mow, V.C., 1999. Contact analysis of biphasic transversely isotropic cartilage layers and correlation with tissue failure. Journal of Biomechanics 32, 1037–1047.

Eijden, T.M.V., Kouwenhoven, E., Verbug, J., Weijs, W.A., 1986. A mathematical model of the patellofemoral joint. Journal of Biomechanics 19, 219–229.

Fairbank, P.G., 1948. Knee joints changes after meniscectomy. Journal of Bone and Joint Surgery 52, 564.

Fithian, D.C., Kelly, M.A., Mow, V.C., 1990. Material properties and structure-function relationship in the menisci. Clinical Orthopedic Related Research 252, 19–31.

Flory, P.J., 1961. Thermodynamic relations for high elastic materials. Transactions of the Faraday Society 57, 829–838.

Fox, R., Harner, C., Sakane, M., Carlin, G., Woo, S.L.-Y., 1998. Determination of the in situ forces in the human posterior cruciate ligament using robotic technology. American Journal of Sports and Medicine 26, 395–401.

Fu, F., Bennett, C., Lattermann, C., Ma, C., 1999. Current trend in anterior cruciate ligament reconstruction. Part 1: biology and biomechanics of reconstruction. American Journal of Sports and Medicine 27, 821–830.

Fukubayashi, T., Kurosawa, H., 1980. The contact area and pressure distribution pattern of the knee. Acta Orthopaedics Scandinavian 51, 871–879.

Fung, Y.C., 1993. Biomechanics. Mechanical Properties of Living Tissues. Springer, Berlin.

Gabriel, M., Wong, E., Woo, S.L.-Y., Yagi, M., Debski, R., 2004. Distribution of in situ forces in the anterior cruciate ligament in response to rotatory loads. Journal of Orthopaedics Research 22, 85–89.

Gardiner, J., Weiss, J., 2003. Subject-specific finite element analysis of the human medial collateral ligament during valgus knee loading. Journal of Orthopaedics Research 21, 1098–1106.

Gardiner, J., Weiss, J., Rosenberg, T., 2001. Strain in the human medial collateral ligament during valgus lading of the knee. Clinical Orthopaedics and Related Research 391, 266–274.

Heegard, J., Leyvraz, P.F., Curnier, A., Rakotomana, L., Huiskes, R., 1995. The biomechanics of the human patella during passive knee flexion. Journal of Biomechanics 28, 265–1279.

Hibbit, Karlsson and Sorensen, Inc., 2004. Abaqus user's guide, v. 6.4. HKS inc. Pawtucket, RI, USA.

Hirokawa, S., Tsuruno, R., 2000. Three-dimensional deformation and stress distribution in an analytical/computational model of the anterior cruciate ligament. Journal of Biomechanics 33, 1069–1077.

Holzapfel, G.A., 2000. Nonlinear Solid Mechanics. Wiley, New York.

Hull, M.L., Berns, G., Varma, H., Patterson, A., 1995. Strain in the medial collateral ligament of the human knee under single and combined loads. Journal of Biomechanics 29, 199–206.

Jalani, A., Shirazi-adl, A., Bendjaballah, M.Z., 1997. Biomechanics of human tibio-femoral joint in axial rotation. Knee 4, 203–213.

Kawada, T., Abe, T., Yamamoto, K., Hirokawa, S., Soejima, T., Tanaka, N., Inoue, A., 1999. Analysis of strain distribution in the medial collateral ligament using a photoelastic coating method. Medical Engineering and Physics 21, 279–291.

LeRoux, M.A., Setton, L.A., 2002. Experimental and biphasic FEM determinations of the material properties and hydraulic permeability of the meniscus in tension. ASME Journal of Biomechanical Engineering 124, 315–321.

Lewis, J.L., Lew, W.D., Hill, J.A., Hanley, P., Ohland, K., Kirstukas, S., Hunter, R.E., 1989. Knee joint motion and ligament forces before and after ACL reconstruction. ASME Journal of Biomechanical Engineering 111, 97–106.

Li, G., Gil, J., Kanamori, A., Woo, S.L., 1999. A validated three-dimensional computational model of a human joint. ASME Journal of Biomechanical Engineering 121, 657–662.

Li, G., Lopez, O., Rubash, H., 2001. Variability of a three-dimensional finite element model constructed using magnetic resonance images of a knee for joint contact stress analysis. ASME Journal of Biomechanical Engineering 123, 341–346.

Limbert, G., Middleton, J., Taylor, M., 2004. Finite element analysis of the human ACL subjected to passive anterior tibial loads. Computer Methods in Biomechanics and Biomedical Engineering 7, 1–8.

Macnicol, M.F., Thomas, N.P., 2000. The knee after meniscectomy. Journal of Bone and Joint Surgery 82-B, 157–159.

Murakami, T., 1990. The lubrication in natural synovial joints and joint prostheses. JSME International Journal 33, 465–474.

Peña, E., Martinez, M., Calvo, B., Palanca, D., Doblaré, M., 2005. Finite element analysis of the effect of meniscal tears and meniscectomy on human knee biomechanics. C Biomechanics 20, 498–507.

Périé, D., Hobatho, M.C., 1998. In vivo determination of contact areas and pressure of the femorotibial joint using nonlinear finite element analysis. Clinical Biomechanics 13, 394–402.

Pioletti, D., Rakotomanana, L., Benvenuti, J.-F., Leyvraz, P.-F., 1998. Viscoelastic constitutive law in large deformations: application to human knee ligaments and tendons. Journal of Biomechanics 31, 753–757.

Proctor, C.S., Schmidt, M.B., Kelly, M.A., Mow, V.C., 1989. Material properties of the normal medial bovine meniscus. Journal of Orthopaedics Research 7, 771–782.

Sathasivam, S., Walker, P.S., 1997. A computer model with surface friction for the prediction of total knee kinematics. Journal of Biomechanics 30, 177–184.

Song, Y., Debski, R., Musahl, V., Thomas, M., Woo, S.L.-Y., 2004. A three-dimensional finite element model of the human anterior cruciate ligament: a computational analysis with experimental validation. Journal of Biomechanics 37, 383–390.

Spilker, R.L., Donzelli, P.D., Mow, V.C., 1992. A transversely isotropic biphasic finite element model of the meniscus. Journal of Biomechanics 25, 1027–1045.

Suggs, J., Wang, C., Li, G., 2003. The effect of graft stiffness on knee joint biomechanics after ACL reconstruction: a 3D computational simulation. Clinical Biomechanics 18, 35–43.

Vedi, V., Williams, A., Tennant, S.J., Spouse, E., 1999. Meniscal movement. Journal of Bone and Joint Surgery 81-B, 37–41.

Viidik, A., 1990. Structure and function of normal and healing tendons and ligaments. In: Mow, Ratchiffe, Woo (Eds.), Biomechanics of Diarthorial Joints. Springer, New York.

Walker, P.S., Erkman, M.J., 1975. The role of the menisci in force transmission across the knee. Clinical Orthopaedics and Related Research 109, 184–192.

Weiss, J., Gardiner, J.C., 2001. Computational modelling of ligament mechanics. Critical Reviews in Biomedical Engineering 29, 1–70.

Weiss, J., Maker, B., Schauer, D., 1995. Treatment of initial stress in hyperelastic finite element models of soft tissues. In: Beaver Creek, C. (Ed.), ASME Summer Bioengineering Conference.

Weiss, J., Maker, B., Govindjee, S., 1996. Finite element implementation of incompressible, transversely isotropic hyperelasticity. Computer Methods and Applications in Mechanical Engineering 135, 107–128.

Weiss, J., Gardiner, J.C., Bonifasi-Lista, C., 2002. Ligament material behavior is nonlinear, viscoelastic and rate-independent under shear loading. Journal of Biomechanics 35, 943–950.

Woo, S.L.-Y., Debski, R., Withrow, J., Janaushek, M., 1999. Biomechanics of the knee ligaments. American Journal of Sports and Medicine 27, 533–543.

Yagi, M., Wong, E., Kanaromi, A., Debski, R., Fu, F., Woo, S.L.-Y., 2002. Biomechanical analysis of an anatomic anterior cruciate ligament reconstruction. American Journal of Sports and Medicine 30, 660–666.

Yamamoto, K., Hirokawa, S., Kawada, T., 1998. Strain distribution in the ligament using photoelasticity. A direct application to the human ACL. Medical Engineering and Physics 20, 161–168.